Indian Journal of Pure & Applied Physics
Vol. 59, September 2021, pp. 603-611

Indigenously Designed and Fabricated Mechanical Milling set-up to Synthesis Nanoparticles: A Cost-effective Method

Chetan Chavan[a], Rajashekhar Fakeerappa Bhajantri[a]*, Soumya Siddalingappa Bulla[a,b] & Kathiresan Sakthipandi[c]*

[a]Department of Studies in Physics, Karnatak University, Dharwad, Karnataka 580 003, India
[b]Department of Studies in Physics, Davangere University, Shivagangotri, Davangere, Karnataka 577 007, India
[c]Department of Physics, SRM TRP Engineering College, Tiruchirappalli, Tamil Nadu 621 105, India

Received 3 July 2021; accepted 11 August 2021

In recent days, the area of nanomaterial synthesis has been very attractive due to the distinguished physicochemical properties which can be modified with a different nanostructure and morphology. In this present investigation, a simple and unique approach on fabrication and testing of homemade ball milling has been developed for laboratory use. In the set-up, the gears have been used to provide positive drive over the container by meshing teeth with driver and driving shaft. Just by changing the position of gears horizontally, the different sized container can be mounted for the same set-up based on the requirement. Container was made of stainless-steel metal; it was then threaded on both sides to suit the stainless-steel caps using a lath system and made easy for cleaning container. Reduction of size of the Fe_2O_3 particles was achieved in short period of time. The particle size of pure and ball milled samples from scanning electron microscope was 227-36 nm. Whereas, the particle analyzer measurement shows that particle size ranges from 230-22 nm.

Keywords: Ball milling, Nanoparticles, Cost-effective, Gears, Zeta potential.

1 Introduction

Mechanochemistry has been well established for the mineral extraction in material science and chemistry. This process involves the nature of reaction and frequency of solids caused by the incorporation of mechanical energy with the samples such as grinding using a mortar and pestle. The traditional system of metals extraction from minerals were initiated long ago during the early stage of evolution of chemistry[1-3] that involves some practices of mechanical character ameliorating the approachability of the fine powder. The typical speed of traditional ball milling was 30 - 150 rotations per minute (RPM). However, the limited chemical reactions were successfully carried out by grinding due to its low grinding strength and speed. Generally, one can expect fine and better quantity milling in lesser time. To overcome this limitation associated ball-milling, a planetary mill (mixer mill) has been developed.[4] Further, the planetary milling accounts for up to 30% of power consumption in mineral operations. Planetary milling has smaller chamber balls and limited capacity.

Various processes take place during mechano-chemical procedure such as the reduction of particle size,[2,5] the generation of new surfaces,[6,7] point defects and dislocations[8] in the crystalline structure and polymorphic transformations.[2,9] The equipment used for characteristically mechanical activation includes the retschmill,[9] tumbling mill,[9] stirring (attritor) ball mill,[8-10] vibration mill,[9] pin mill,[8,9] rolling mill,[8,9] and planetary ball mill.[9,11] Recent innovative procedures in mechanochemistry are more ecofriendly and have many advantages over the traditional ones.[12] Ball milling process is an original strategy to modify materials at the nanometer scale.[13] Particle size reduction, increase of specific surface area, crystalline structure decomposition and bond breakage have been identified as the main process during ball milling process.[9]

A variety of nanoparticles were fabricated by top-down approaches like mechanical milling, etching, laser ablation, sputtering and electro-explosion.[14] This top-down technique has been used as a simplest way to synthesis a variety of nanomaterials such as metal oxides,[15-17] carbon materials,[15,18] zeolites,[15,19] and metal organic frame works.[15] Ball-milling is a well-established method for obtaining fine particles with high surface area from bulk materials.[20] Grinding method or ball milling is used to grind the

*Corresponding Author:
(Email: rfbhajantri@kud.ac.in, sakthipandi@gmail.com)

microparticles into enormously fine powders. During this milling process, the collision or impact rate between the rigid tiny balls in a concealed container will generate localized high pressure which determines the nanostructures of the materials. In addition, ball milling is a simple technique used for nanoparticle synthesis as it is a time-convenient, one - step synthesis, enabling us to work under environment – friendly, waste-free conditions and it influences the reactivity by creating interphases (especially in composite and multi or phase systems)[21] and its mechanism includes diffusion improvement strain generation, structural, electronic and ionic defects.[5]

Depending on the applications, there are different types of ball mill that are commercially available in market. With the covid-19 pandemic having engulfed the globe; the government authorities have found it difficult to provide funds for research activities of other fields. In such times of economic crisis, this home-made milling experimental set-up comes handy as it is economical as well as effective to synthesize the different nanostructures.

Therefore, in this investigation, an approach was made to design and fabricate low-cost milling method from locally available materials. A unique and simple model was designed and fabricated to work continuously and to examine how effectively size of the sample reduces at room temperature. This provides a possibility to construct future laboratory devices which produce the nanomaterials through top-down approach. Therefore, the present investigation is aimed to fabricate low-cost ball milling that can grind sample to fineness powder (nm). Materials used for the fabrication were commonly available in the market. Later, the changes are remarked that occurred when the sample was ball milled with both sliding and cascading effects. This study is validated by examining the improvements when a lifting bar is attached to the container. This design helped to improve the workability of the whole system. Further, nano Fe_2O_3 nanoparticles were synthesized from designed experimental facility.

2 Experimental Details

2.1 Design and fabrication

The indigenously design and fabrication of milling machine is made on the platform of acrylic sheet (M/s. Chochen Industry Co. Ltd. Cast Acrylic sheet) and the dimension of the platform is 400 ×180 × 11.93 mm^3. The materials used for fabrication of the ball milling were shown in Fig. 1. The excellent insulating properties and higher surface resistivity of acrylic sheet makes the comfort platform for low-cost ball milling machine. In order to arrest the vibration and heat, two acrylic sheets with dimension of 125 × 50 × 12 mm^3 were prearranged as a base and a 1000 RPM DC motor (M/s. Johnson's gear, India) is screwed and uplifted with the acrylic platform by using the side shaft motor L-shaped clamp. Two pair of mounting ball bearings made of zinc alloy with bore diameter 8 mm were installed with proper alignment on the base platform as shown in Fig. 1. Stainless steel driving axle and driven axle shaft were embedded through the mountain ball bearings and gears. The gears were fixed as convenient to the sample container. Washers were stacked on the outer lips of the driving and driven gears. They were used to avoid missing of the positive drive. Driving shaft axle of length 27 mm and diameter of 8 mm was fastened to DC motor through flexible shaft coupling which is made up of aluminum. Container was made from stainless steel pipe with dimensions of L × D (82 × 22 mm^2), in order to ease the handling of the container, it was threaded on both sides to fit the stainless-steel caps using lath machine. This special arrangement of opening both sides provide easy loading and unloading of samples. Digital non-contact tachometer (M/s. Mextech DT-2234C, with Resolution : 0.1 RPM, Accuracy ±0.05 %, Detecting Distance: 2 to 20 inch.) used to measure RPM. For better understanding about the design of the milling set-up, the 3-D view of the designed set-up was simulated using C-atia V5 Software and the same was shown in Fig. 2. The actual

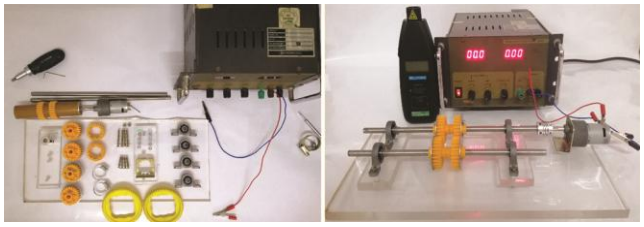

Fig. 1 — Snapshots of the before and after assembling of the Ball-milling

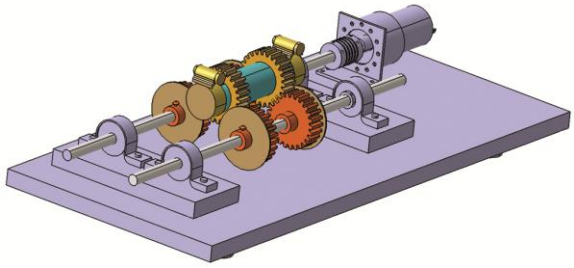

Fig. 2 — 3-D View of Ball-milling using Catia V5 Software

schematic representation of the indigenously designed experimental set-up was represented in Fig. 3. Further, the specifications and cost of the components used to fabricate the experimental set-up was given in Table S1 as a supplementary file.

2.2 Working

DC motor placed horizontally fixed to driving axle was powered by the 12V DC power supply. When the power is transmitted from the motor to driving axle, the driving gear started the rotation. In order to calibrate the RPM, the input voltage is slowly increased, and the rotating RPM was marked. Table 1 and Fig. 4 show the voltage depended on RPM. It is interested to explore that one can obtain the ~350 RPM at lower voltage through this indigenously designed experiment set-up. Then, the stainless-steel container was placed on ball bearing with a teeth arrangement on its girth provides a positive drive by meshing the teeth with identical one. Thus, the container starts rotating at constant speed and incessantly which can be regulated using a power supply. A lifting rod is hooked horizontally along the axial line of the container provides cascading effect. The motion of milling ball depends upon the performance of rotating speed of the container. To increase the rotation speed, ball raises as high as possible and then fall back on the bottom of the jar this causes breakage of the sample. Size reduction in milling occurs as a result of three fragmentation mechanisms *i.e.*, abrasion, cleavage and fracture[20,21]. To carry out the procedure, one should assure the constant operations of DC motor at continuous speed. The variation of the input voltage leads to distinctive change in the RPM. Therefore, this taken care might affect results of the experiment due to varying RPM. Container and stainless-steel balls were washed and dried at 40 °C in hot air oven. Then, container was filled with 25% of stainless-steel balls of different size as per BPR 20:1. The specifications of stainless-steel ball and mass of are as in the below Table 2.

2.3 Validation – Production of Fe_2O_3 nanoparticle

The indigenously designed set-up was validated by preparing Fe_2O_3 nanoparticle. 25% of the container was filled with Fe_2O_3 (M/s. Hi-Media, Mumbai) powder and 40 number of SS balls. Later, the container was closed and placed on the rotating panel. The instrument was powered after rechecking the bolts, nuts and connection. In order to determine the efficiency of the set-up, the ball milled samples were collected in the different intervals of milling such as

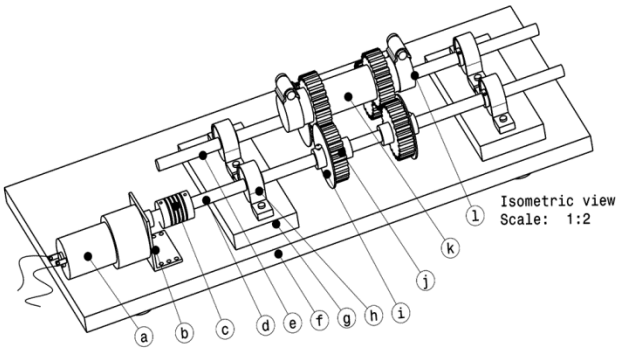

a) 100 Rpm Johnson Gear Dc Motor 12v
b) Side Shaft Motor Clamp(L-Clamp)
c) Shaft Coupling
d) Driving Shaft Axle
e) Driven Shaft Axle
f) Acrylic Sheet Platform
g) Acrylic Sheet Base
h) Mounting Ball Bearing
i) Flat washers
j) Gears
k) Container
l) Container cap

Fig. 3 — Schematic representation of the home-made ball-milling

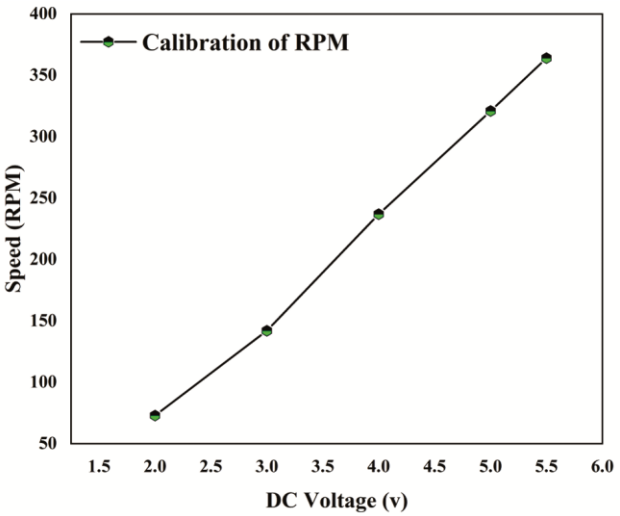

Fig. 4 — Calibration curve of the RPM

Table 1 — Calibration of the RPM

Applied Voltage (volts)	2	3	4	5	5.5
RPM	73	142	237	321	364

Table 2 — Technical specifications of grinding media

Stainless Steel balls Diameter (mm)	No. of balls used (Units)	Total mass of balls (grams)
11.476	1	5.6242
11.053	1	3.5679
7.94	5	7.4003
5.71	5	2.2285
4.79	28	7.1563

0 hr, 1hr, 10 hr, 20 hr and 30 hr and the samples prepared at different milling time were given codes as FEO00 FEO01, FEO10, FEO20 and FEO30 respectively. Attribution of crystal structure of synthesized Fe_2O_3 nanoparticles by powder x-ray diffraction (XRD; M/s. RIGAKU X-ray diffractometer, model-smart lab SE with Cu-Kα source at 2θ, scan range 10° to 90 °, step width-0.01°, scan speed -5.00°/min). Implementing scanning electron microscope (SEM; M/s. Hitachi, S-3400N, Japan) structurally analyzed the surface morphology of Fe_2O_3 nanoparticles. The SEM images were acquired in various magnification and elemental analysis which was conducted by using energy-dispersive X-ray spectroscopy (EDS-Thermo, Noran System 7, USA). Measurements of dynamic light scattering (DLS) were executed employing Microtrac USA, Nanotrac Wave and Model MN401. As the light source, the solid -state laser-diode (wavelength 780 nm, near-infrared, Optical Power: 3Mw nominal, 5 Mw max) has been used. All tests were carried at 25 °C with a suspension viscosity of 0.889 cP. The photodetector sensed scattering light intensity at a scattering angle of 90 °. The sample and the balls were poured on the filtering paper to obtain finest powder at different time intervals and a quite low concentration particles were dispersed and sonicated well using distilled water. The prepared solutions were examined using the particle analyzer.

3 Results and Discussion

3.2 XRD Structural Analysis

Phase formation and purity of pure FEO00 and ball milled FEO01, FEO10, FEO20 and FEO30 samples were investigated from their respective XRD pattern by comparing with the standard JCPDS data (JCPDS # 89-8104) as shown in Fig. 5. The formation of pure Fe_3O_4 phase in both pure FEO00 and ball milled FEO01, FEO10, FEO20 and FEO30 samples has been confirmed by matching their XRD pattern with the standard JCPDS card # 89-8104 of α-Fe_2O_3 having rhombohedral crystal system with $R\bar{3}c$ space group. Presence of major peaks at or around 24.31°, 33.32°, 35.79°, 41.02°, 49.64°, 54.23°, 57.74°, 62.61° and 64.17 ° represents the (0 1 2), (1 0 4), (1 1 0), (1 1 3), (0 2 4), (1 1 6), (0 1 8), (2 1 4) and (3 0 0) crystallographic diffraction planes of α-Fe_2O_3 system. The effect of ball milling on the crystal structure of α-Fe_2O_3 is visible in the magnified view of high intensity peaks, shown in Fig. 6. The noticed higher angle shift in the peaks represent the possible

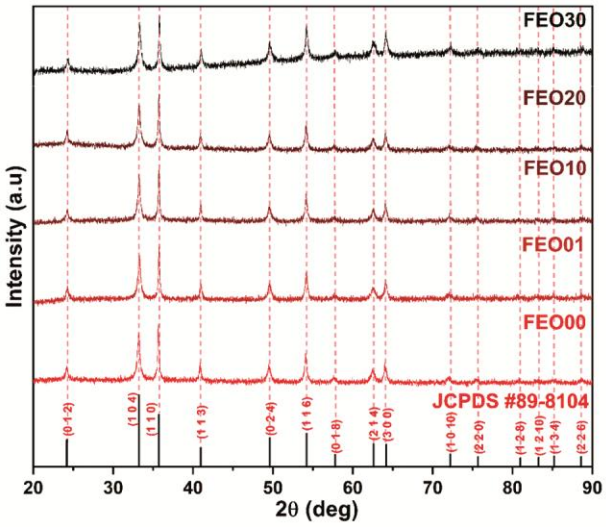

Fig. 5 — XRD patterns of pure and Ball Milled Fe_2O_3 particles

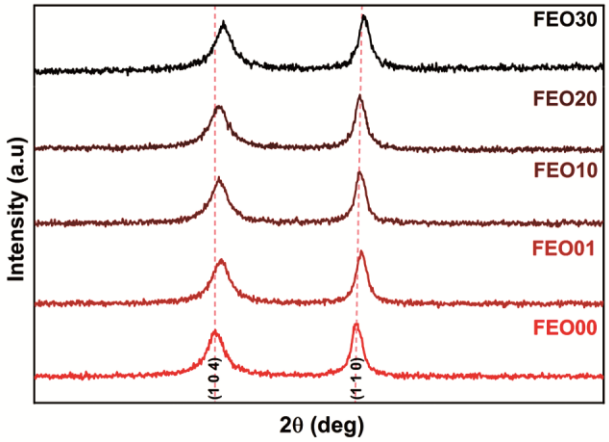

Fig. 6 — Magnified view of XRD patterns of pure and Ball Milled Fe_2O_3 particles

Table 3 — Calculated average crystallite size, dislocation density and micro strain for pure and Ball milled α-Fe2O3.

Sample	Average crystallite size D (nm)	dislocation density $\delta\times10^{-3}$ (nm^{-2})	micro strain $\varepsilon \times 10^{-3}$
FEO00	36.5827	0.74722	3.09406
FEO01	36.2589	0.76063	3.11486
FEO10	31.7866	0.98972	3.11753
FEO20	26.3537	1.43985	3.75995
FEO30	27.605	1.31227	3.58315

modifications in the crystal structure in effect of ball milling. Further, the average crystallite size of α-Fe_2O_3 was calculated using Scherrer's equation[23] and tabulated along with dislocation density[24] and micro strain [24] in Table 3. Defects caused by the mechanical consequences of balls during friction, utilization of higher media surface, *i.e.*, higher powder to ball

weight ratio and vigorous grinding, results in a change in dislocation density and micro strain. Irrespective of milling machinery when Fe_2O_3 is subjected for prolonged grinding, the dislocation density decreases. From Table 3, it is known that the reduction of the Fe_2O_3 micro strain values decreases as the milling time increases.

It is also noted from Table 3 that the crystallite size of the pure FEO00 and ball milled FEO01, FEO10, FEO20 and FEO30 samples were 36.58, 36.25, 31.78, 26.35 and 27.605 nm. The crystallite size was decreased with an increase in milling time. Further, the micro stain and dislocation density were increased with an increase in milling time. However, the crystallite size of FEO30 sample was little increased due to the excess milling time. The milling time dependent crystallite size, dislocation density and micro strain of pure FEO00 and ball milled FEO01, FEO10, FEO20 and FEO30 samples are given in Fig. 7, which confirms that milling of α-Fe_2O_3 around 20 hours gives the minimum in crystallite size and maximum in dislocation density and micro strain.

3.3 SEM analysis

The effect of ball milling on the particle morphology of pure FEO00 and ball milled FEO01, FEO10, FEO20 and FEO30 samples were analyzed from the observed SEM images which are shown in Fig. 8 (a), (d), (g), (j) and (m), respectively. It is observed that the pure FE00 particles possess rod like morphology having average length below 1 μm and diameter in the range up to 400 nm. Few rods-like particles have been attached to one another to form small clusters of Fe_2O_3. Whereas the particle size was decreased in the ball milled FEO01, FEO10, FEO20 and FEO30 samples. Noticeable variations can be

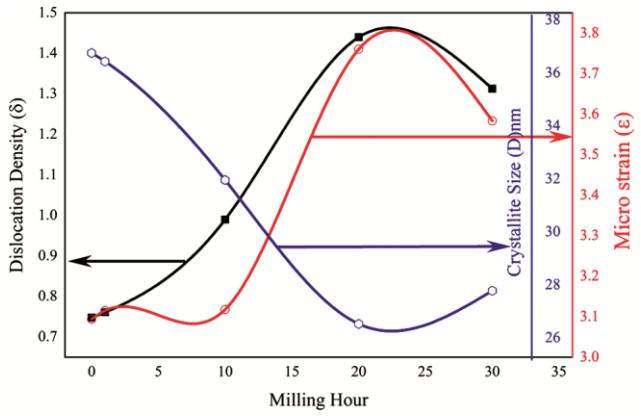

Fig. 7 — The results illustrate that change in Crystallite size, Dislocation density, micro strain, of pure and Ball Milled Fe_2O_3 Particles

observed in the particle morphology with increasing milling time. The length of Fe_2O_3 nanoroads seem to decrease with increasing milling time whereas the average diameter gradually increases from 50 to 100 nm. As a result, with an increasing milling time, the particles slowly converts from rod to nearly spherical morphology. The size distribution histogram of the Fe_2O_3 particles in FEO00, FEO01, FEO10, FEO20 and FEO30 samples are shown in Fig. 8 (b), (e), (h), (k) and (n). In all samples, the approximate diameter of Fe_2O_3 rods ranges from 20 to 400 nm and the average diameter are calculated through Gaussian curve fitting on the size distribution histogram and are found to be 227, 198, 104, 75 and 36 nm respectively. The EDX spectra shown in Fig. 8 (c), (f), (i), (l) and (o) evident the presence of essential elements that are oxygen and iron in all samples.

It ensures that the indigenously designed experimental set-up can be effectively used to reduce the particle size. This confirms the impact collision of the balls and particles during the rotation of sample drum. Evaluated by comparing to another ball mill *i.e.*, Planetary ball mill, High-energy ball milling stainless steel attritor, RETSCH PM400 as commonly identified in the literature refer Table 4. The size distribution pattern was similar with longer milling time, and more crusher ball used could yield fine powder, however our set-up gives optimize performance and particles gradually switching from the rod to almost spherical morphology without spotting impurities.

Table 4 — Correlation of present set-up with commercially available ball mills

Number of Hours Milling	Size of Particle	rpm	Ball Mill Type	Ref
Sample: - α-Fe_2O_3				
	XRD			
15 h	34.64 nm	250 rpm	Planetary ball mill	25
30 h	23.16 nm			
45 h	18.46 nm			
Sample: - α-Fe_2O_3 Powder (1 μm)				
	XRD			
10 h	41.2 nm	300 rpm	High-energy ball milling stainless steel attritor	26
80 h	23.3 nm			
100 h	11.5 nm			
	(TEM)			
100 h	15 nm			
Sample: - α-Fe_2O_3 Powder (50 nm)				
	XRD	400 rpm	RETSCH PM400	27
12 h	28nm			

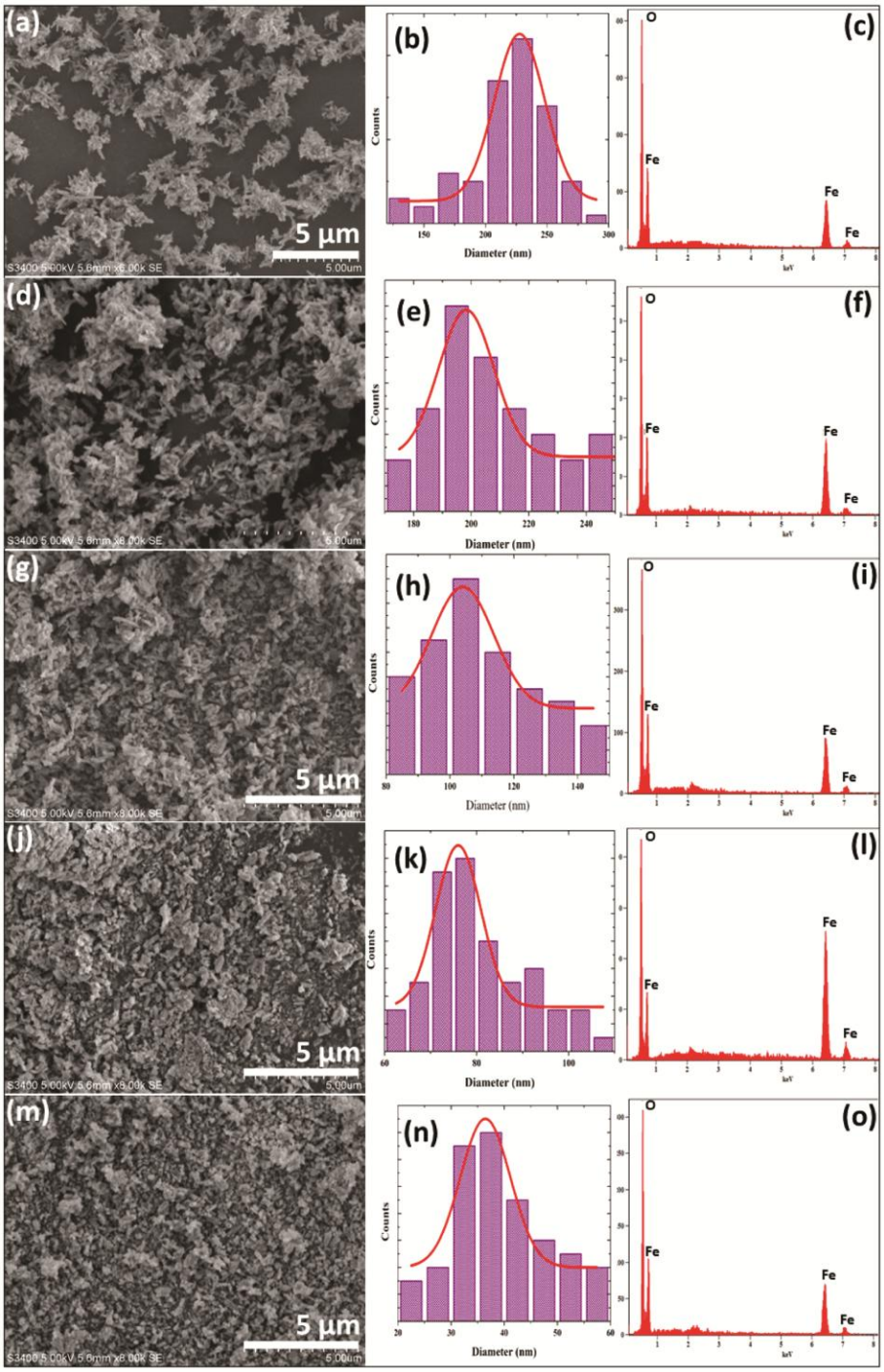

Fig. 8 — SEM images of (a) FEO00, (d) FEO01, (g)FEO10, (j) FEO20 and (m) FEO30 samples respectively along with their size distribution histogram (b), (e), (h), (k) and (n) and EDX spectra (c), (f), (i), (l) and (o)

3.4 DLS analysis

DLS was another approach included in material science to verify the size distribution profile of small particles in suspension and even polymer solution. In order to further validate the particle size of synthesized Fe_2O_3 nanoparticles, the average particle size were again characterized through photon correlation spectroscopy that is DLS measurement. In the dilute suspension, the nanoparticles experience Brownian motion, which generates temporal fluctuations in the dispersed light intensity. Autocorrelation between the two is being evaluated in

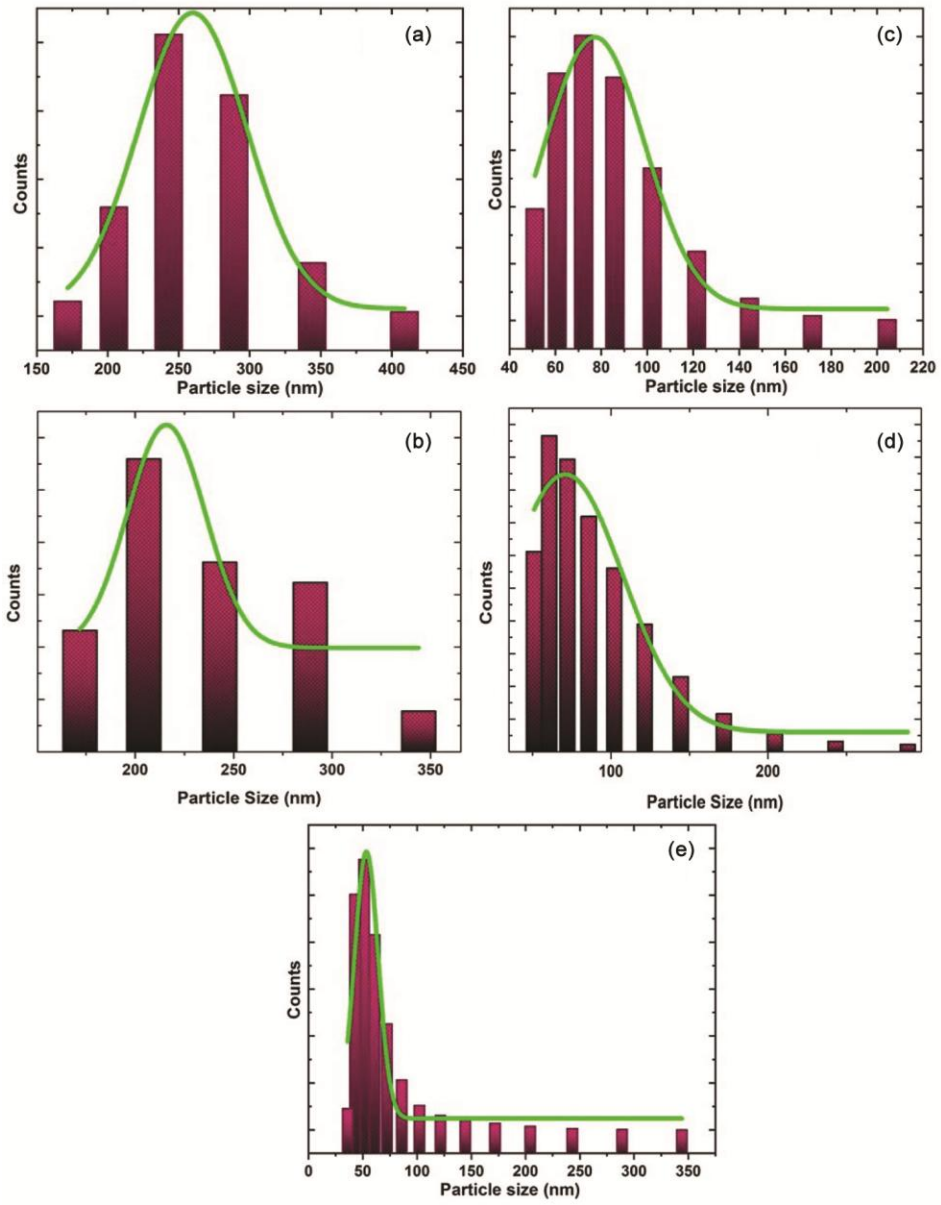

Fig. 9 — Particle size distribution histogram measured during zeta potential measurement. (a) FEO00, (b) FEO01, (c) FEO10, (d) FEO20 and (e) FEO30

order to determine the average translational diffusion coefficient D which could also be used to obtain the average hydrodynamic radius R_H using Stokes - Einstein equation $D=k_bT/6\pi\eta R_H$ where k_b is Boltzmann constant, T is temperature of suspension, and η is the viscosity of surrounding media[28].

A quite low concentration particles were diluted and sonicated well using distilled water. For zeta potential (ZP) measurement, diluted samples were taken in a syringe and properly loaded in the cuvette. The surface charge and size distribution of prepared FEO00, FEO01, FEO10, FEO20, and FEO30 samples were measured using ZP analyzer and the obtained particle size distribution is shown in Fig. 9, as a histogram. It is found that the size distribution of ball milled samples range from ~ 15 to 400 nm. For unmilled FE00 sample, the majority of the particle have size in the range of 200 to 350 nm whereas, FEO01, FEO10, FEO20 and FEO30 samples are in the range from 100 to 300 nm, 50 to 120 nm, 50 to 100 nm, and 18 to 36 nm respectively. The average particle size of FEO00, FEO01, FEO10, FEO20 and FEO30 are found to be 230 nm, 215 nm, 77 nm, 67 nm, and 22 nm respectively, as measured from the

Gaussian curve fitting on the size distribution histogram. The outcome of these results lead to the conclusion that the DLS measurements of the ball milled Fe_2O_3 nanoparticles for extended timeframes show a reduction in particle sizes. This is comparatively in close agreement with the SEM measurements.

ZP is a function of surface charge phenomenon that arises when some material is placed in liquid, and it is an important parameter for estimating and controlling dispersion stability. The magnitude of the recorded ZP is a sign of the repulsive force present and can be used to estimate long-term stability. When the suspension particles have a significant negative or positive ZP then they seem to repel each other so there is no tendency for the particles to come together. However, if the particles contain small ZP values, there is no force to show the particles coming together and flocculating. In the case of FEO00 particles possess positive polarity on the surface with ZP value of 0.1 mV. When the particle is subjected for milling, we observed change in ZP values for FEO01, FEO10, FEO20, and FEO30 are as follows 2.5 mV, 6.5 mV, 48.4 mV, and 5.6 mV, respectively. Meanwhile it was noted that there was no change in polarity in milled samples. The conductivity was measured as 63 μS cm^{-1} with field strength of 5 kV m^{-1} for FEO00, The increasing trend in conductivity and the strength of the field were evidenced for 1hr, 10hr, 20hr, 30hr, and are obtained to be 27,367 μS cm^{-1} with 0.7 kV/ m, 530 μS cm^{-1} with field strength of 5 kV m^{-1}, 18,048 μS cm^{-1} with field strength of 0.8 kV m^{-1} , 272 μS cm^{-1} with field strength of 5.0 kV m^{-1} respectively as the ball milling time increases. ZP measurements offer clear insight into the factor that can influence dispersion stability, aggregation or flocculation etc. Interestingly, in most of the cases significant increase in the ZP value was observed with increasing ball milling time. It ensures that the potential to agglomerate particles after prolonged milling is low since the ZP values are high. Above all, by this validation, the effectiveness of the indigenously designed and fabricated mechanical milling set-up is a cost-effective method to synthesis nanoparticles.

4 Conclusions

A different way of the fabrication, processing and validating of home-made indigenous ball milling has been estimated successfully using inexpensive and commonly available raw materials such as gears, which can transmit the rotational motion to different axis, and they can increase or decrease the speed of rotation. The present set-up can be used to maintain gears avoiding overflow from rotating path with the container for easy loading and unloading of sample and can maintain container clean. The outcome of the product. i.e., Fe_2O_3 has been milled for different hours and characterized by Particle analyzer, SEM, XRD. There was decrease in size of particles and particles eventually change from the rod to almost spherical shape. Merits of the present work are increase product yield (by increasing yield and/or selectivity), speed-up the reaction rate and therefore increase the space-time yield, Low-cost investment, the procedure is simple, easy to handle. Hence, the developing and underdeveloped laboratories which have limited resources can make use of the fabricated portable low-cost instrument which was reported in this work for the novel synthesis of nanostructure.

Acknowledgement

With respect and admiration for providing UGC-JRF/SRF support (518772 / Dec 2015), Author Chetan Chavan thanks to University Grants Commission (UGC), New Delhi. Also, one of the author Soumya S Bulla acknowledges the monetary support granted by Karnatak University in the form of University Research Studentship Including Department of Science and Technology, Karnataka Government, India for the award of KSTePS Research Fellowship (DST/ KSTePS / Ph. D. Fellowship / PHY-04:2018-19). This work is also jointly supported by Davangere University. All profound gratitude goes for the experimental facilities provided by the USIC & SAIF (University Scientific Instrumentation Centre) (Sophisticated Analytical Instrument Facility), Karnatak University, Dharwad. A heartfelt thanks to Chethan Raj B, Assistant Professor, GFGC Mudalagi for his support. The authors also acknowledge Science and Engineering Research Board, Department of Science and Technology, Government of India, New Delhi for the research project (SB/EMEQ-089/2013). The authors are grateful to UGC, New Delhi for SAP-CAS Phase-II programme (F.530/9/CAS-II/2015 (SAP-I) for providing financial assistance. The authors are also thankful to Karnataka State Higher Education Council, Govt. of Karnataka for RUSA1.0 grant (KSHEC/254/KUD/15-16/544) at K.U. Dharwad.

References

1 Kuo C L, Lee S & Hwang G S, *Phys Rev Lett*, 100 (2008) 1.
2 Mohammadnejad S, Provis J L & Van D J S J, *Miner Eng*, 52 (2013) 31.

3 Lin I J, *J Therm Anal Calorim*, 52 (1998) 453.

4 Ranu B C, Chatterjee T & Mukherjee N, Ball Milling Towards Green Synthesis Applications Projects Challenges (Published by the Royal Society of Chemistry, From Book Series: Green Chemistry Series), eISBN: 978-1-78262-198-0, (2015) 1.

5 Kumar M, Xiong X, Wan Z, Sun Y, Tsang D C W, Gupta J, Gao B, Cao X, Tang J & Ok Y S, *Bioresour Technol*, 312 (2020) 1.

6 Liang B, Ma J, Su X, Yang C, Duan H, Zhou H, Deng S, Li L & Huang Y, *Ind Eng Chem Res*, 58 (2019) 9030.

7 Da Silva K L, Menzel D, Feldhoff A, Kübel C, Bruns M, Paesano A, Düvel A, Wilkening M, Ghafari M, Hahn H, Litterst F J, Heitjans P, Becker K D & Šepelák V, *J Phys Chem C*, 115 (2011) 7209.

8 Baláž P, Achimovičová M, Baláž M, Billik P, Cherkezova-Zheleva Z, Criado J M, Delogu F, Dutková E, Gaffet E, Gotor F J, Kumar R, Mitov I, Rojac T, Senna M, Streletskii A & Wieczorek-Ciurowa K, *Chem Soc Rev*, 42 (2013) 7571.

9 Tan Q & Li J, *Environ Sci Technol*, 49 (2015) 5849.

10 De S, Joó F, Horváth H, Udvardy A & Czégéni C E, *J Organomet Chem*, 918 (2020) 1.

11 Othman A R, Sardarinejad A & Masrom A K, *Int J Adv Manuf Technol*, 76 (2015) 1319.

12 Boldyrev V V, *Russ Chem Rev*, 75 (1993) 2029.

13 Cantarella M, Gorrasi G, Di Mauro A, Scuderi M, Nicotra G, Fiorenza R, Scirè S, Scalisi M E, Brundo M V, Privitera V & Impellizzeri G, *Sci Rep*, 9 (2019) 1.

14 Khanna P, Kaur A, Goyal D & *J Microbiol Methods*, 163 (2019) 1.

15 Namba S, Takagaki A, Jimura K, Hayashi S, Kikuchi R & Ted O S, *Catal SciTechnol*, 9 (2019) 302.

16 Cheng X, Fabbri E, Kim B, Nachtegaal M & Schmidt T J, *J Mater Chem A*, 5 (2017) 13130.

17 Horie H, Iwase A & Kudo A, *ACS Appl Mater Interfaces*, 7 (2015) 14638.

18 Jeon I Y, Choi H J, Jung S M, Seo J M, Kim M J, Dai L & Baek J B, *J Am Chem Soc*, 135 (2013) 1386.

19 Kurniawan T, Muraza O, Miyake K, Hakeem A S, Hirota Y, Al-Amer A M & Nishiyama N, *Ind Eng Chem Res*, 56 (2017) 4258.

20 Hong W X, *Mech Syst Des*, (2016) 1.

21 Piras C C, Fernández-Prieto S & De Borggraeve W M, *Nanoscale Adv*, 1 (2019) 937.

22 Varinot C, Hiltgun S, Pons M N & Dodds J, *Chem Eng Sci*, 52 (1997) 3605.

23 Kulandaivelu P, Sakthipandi K, Senthil Kumar P & Rajendran V, *J Phys Chem Solids*, 74 (2013) 205.

24 Ayed R B, Ajili M, Garcia J M, Ziouche A, Kramer J L C & Turki N K, *Optik*, 219 (2020) 1.

25 Shilpa C, Deepa C, Aishwariya R, N P, Chaitra V & Venkatraman U, *Int J Chem Tech Res*, 7 (2015) 1098.

26 Lee J S, Lee C S, Oh S T & Kim J G, *Scr Mater*, 44 (2001) 2023.

27 Alizadeh M, Hosseini S A, Nouri S M M, Khalighi Z & Delfarah B, *Chem Eng Commun*, 205 (2018) 1.

28 Sharma P, Dhiman S, Kumari S, Rawat P, Srivastava C, Sato H, Akitsu T, Kumar S, Hassan I & Majumder S, *Mater Res Express*, 6 (2019) 1.